Noname manuscript No.
(will be inserted by the editor)

Physical models of infant mortality. Implications for defects in biological systems

Alex Bois [1] · **Eduardo M. García-Roger** [2] · **Elim Hong** [3] · **Stefan Hutzler** [*4] · **Ali Irannezhad** [4] · **Abdelkrim Mannioui** [1] · **Peter Richmond** [4] · **Bertrand M. Roehner** [5] · **Stéphane Tronche** [1]

Received: date / Accepted: date

Abstract Reliability engineering concerned with failure of technical inanimate systems usually uses vocabulary and notions of human mortality, e.g. infant mortality vs. senescence mortality. Yet few data are available to support such a parallel description. Here we focus on early stage (infant) mortality for two inanimate systems, incandescent light bulbs and soap films, and show the parallel description is clearly valid. Theoretical considerations of the thermo-electrical properties of electrical conductors allows us to link bulb failure to inherent mechanical defects. We then demonstrate the converse, that is, knowing the failure rate for an ensemble of light bulbs, it is possible to deduce the distribution of defects in wire thickness in the ensemble. Using measurements of lifetimes for soap films we show how this methodology links failure rate to geometry of the system; in the case presented this is the length of the tube containing the films. In a similar manner, for a third example, the time-dependent death rate due to congenital aortic valve stenosis is related to the distribution of degrees of severity of this condition, as a function of time. The results not only validate clearly the parallel description noted above, but point firmly to application of the methodology to humans, with the consequent ability to gain more insight into the role of abnormalities in infant mortality.

Keywords Congenital malformations · infant mortality · aortic valve stenosis · failure rates · defect distributions · soap film lifetime experiments

* Corresponding author, E-mail: stefan.hutzler@tcd.ie
[1] Aquatic Facility, Pierre and Marie Curie Campus, Sorbonne University, Paris, France.
[2] Institut Cavanilles de Biodiversitat I Biologia Evolutiva, University of València, València, Spain.
[3] Neuroscience Laboratory, Sorbonne University and INSERM (National Institute for Health and Medical Research), Paris, France.
[4] School of Physics, Trinity College Dublin, Dublin, Ireland.
[5] Institute for Theoretical and High Energy Physics (LPTHE), Pierre and Marie Curie campus, Sorbonne University, Centre de la Recherche Scientifique (CNRS), Paris, France.

1 Introduction: parallels between lifetimes of technical and living systems

The age-dependent mortality rates for humans and other animal species have a declining part, corresponding to infant mortality, which is followed by a rising part, corresponding to the ageing process [1–3]. Technical systems are said to show a similar pattern, although little published empirical evidence appears to exist to support the point. Many publications feature stylized reliability curves instead of actual data. This lack of empirical evidence led us to develop our own simple physical models of living systems[1].

Reliability engineers distinguish three phases in the working life of technical devices. First, the initial or 'burn-in' phase, where manufacturing defects can cause items to fail. As they are progressively eliminated the failure rate falls. This is followed by a 'normal' or working phase where the failure rate is low and roughly constant. Finally comes the 'ageing' or wear-out phase, during which the failure rate increases until eventually all devices in the sample have failed. This process also describes quite well the behaviour of the mortality for living systems, except in living systems the ageing phase follows almost immediately the infant mortality phase. There seems to be no substantial working phase in living systems where the death rate remains constant. However, although the three phases described above are a fairly natural conjecture, published technical data supporting the description is noticeable by its absence.

One may speculate as to why this is so. Perhaps, since for all technical devices the failure rates are low, generating data which yield accurate results for this quantity would require large numbers of devices being monitored over long periods of time. Such assays would take many years and are likely to be expensive. Therefore they are usually limited to crucial devices, such as items destined for the space industry, and the results are not normally made public[2]. An exception appear to be computer hard drives, for which failure data is now available online[3]. In the case of fluorescent light bulbs, which have average lifetimes of about 20,000 hours, rapid on-off switching cycles, which result in a lifetime decrease, provide an alternative testing method [4,5].

Planned obsolescence, or designing products to have a shorter service-life than would otherwise be possible, is another plausible reason for the lack of published data. Although claims of planned obsolescence have often been made by consumer associations, they are usually denied by companies. An exception is the case of incandescent light bulbs where there is convincing evidence. In Krajewski [6] there is a detailed account of how in the 1920s major producers

[1] We use the term "model" with the meaning of a convenient analogy of a real - in this case, living - system. Only once the mechanism of ageing is better understood will it be possible to formulate a mathematical model.

[2] The much publicized investigation by Richard Feynman of the O-ring failure which led to the Challenger space shuttle catastrophe illustrates that even here failure of the components was not fully understood. For a video showing Feynman's demonstration see https://www.youtube.com/watch?v=raMmRKGkGD4.

[3] The data is provided by the storage provider Backblaze, see https://www.backblaze.com/blog/how-long-do-disk-drives-last/.

formed an international cartel with the purpose of limiting the life span of light bulbs to 1,000 hours. In his study the author shows that in Germany between 1926 and 1933 the average life of light bulbs fell from 1,800 hours to 1,200 hours. Under such circumstances life span statistics clearly become irrelevant.

The focus of the present paper is the initial variation of failure/mortality rates. Our aim in particular is to find a mechanism that explains the occurrence of an infant mortality phase in living beings. To this end, in this paper we will make use of inanimate technical systems, namely light bulbs and soap films, whose "burn in" phases resemble infant mortality, and for which it is important to recognize that

- the impact of a manufacturing defect does not necessarily appear immediately after the device starts to work; it can appear a long time later,
- in principle, as we show below, there is a close connection between the nature and severity of defects and the time to failure.

To illustrate this, we will, following a brief section on definitions and terminology, start by introducing a simple model for failure in light bulbs, based on well-known properties of electrical circuits. We then develop a methodology for predicting manufacturing defects from failure rate curves. In order to test the validity of our approach we need access to empirical data. As noted above, light bulbs are not a convenient system in this regard. We have instead carried out experiments with soap films which have only recently been introduced for the study of ageing and failure [7].

Here the complexity of the factors determining film lifetime (e.g. physical, chemical, environmental factors) does not allow for the development of a simple toy model for film stability. However, our experiments identify experimental parameters which control film lifetime and which can be used to analyze failure rates.

Finally, we apply our method of relating the distribution of defects to lifetime data to an example from human biology, by examining the temporal variation of the death-rate from congenital stenosis of the aortic valve.

Recently, Nee [8] has suggested that manufacturing/congenital defects may not be the only cause for the specific variation of failure or mortality rates. The sudden malfunctioning of a technical device, or a sudden death, may result from the deterministic behaviour of a system whose dynamics allows for chaotic behaviour. So called strong-chaos, which can be generated via the logistic map, can be associated with type II survivorship curves, i.e. constant mortality rates (see Section 2). Weak chaos on the other hand, which features periods of stability, interrupted by chaotic bursts, can be mapped to decreasing infant mortality (type III survivorship). Chaotic activity has indeed been observed in both human cardiac data, as well as in brain signals, where it might be associated with epilepsy, rendering relevance to Nee's scenarios.

In this paper, however, we will focus on the role that well defined manufacturing or congenital defects play for the 'burn-in' phase or infant mortality.

2 Definitions and terminology

The study of lifetime statistics features in a range of subject areas, such as biology, engineering, or actuarial science. Although the underlying mathematical concepts are shared, the use of different terminologies can lead to confusion. We will for this reason briefly introduce the key concepts here, which will be used throughout the text.

Given a population of size N, which could be made up of humans, light bulbs, soap films, etc, we wish to describe its evolution as a function of time t. A *survival* or *reliability function* $s(t)$ is defined as

$$s(t) = N(t)/N(t=0), \tag{1}$$

where $N(t)$ is the number of members in the population that is still alive/intact at time t. The function $s(t)$ decreases with time from its initial value $s(0) = 1$, to zero, when all members have "died". The *failure function* $f(t)$ is defined as its complement, $f(t) = 1 - s(t)$.

The failure function may also be introduced via a *failure density function* $f_T(t)$ as

$$f(t) = \int_0^t f_T(t)dt. \tag{2}$$

Here $f_T(t)dt$ is the probability of failure in the time interval $[t, t+dt]$.

Writing the reliability function $s(t)$ as $s(t) = 1 - \int_0^t f_T(t)dt$, we obtain

$$f_T(t) = -ds(t)/dt. \tag{3}$$

We shall use this relation when discussing our soap film data in section 4.

Often failure data is displayed in the form of a *failure rate* $\mu(t)$ (also called hazard function (reliability theory), or force of mortality (actuarial science))[9]. This function is defined as

$$\mu(t) = -\frac{1}{s(t)}\frac{ds(t)}{dt} = -\frac{d\ln s(t)}{dt}, \tag{4}$$

i.e. $\mu(t) = \frac{f_T(t)}{s(t)}$. For short times, when $s(t) \simeq 1$, one thus obtains $\mu(t) \simeq f_T(t)$.

In ecology, graphs using a logarithmic scale for $s(t)$ as a function of (linear) time are called *survivorship curves*. A straight line in such a graph (i.e. $\mu(t) = const.$) is referred to as type II survivorship curve. An accelerating decay of $\log s(t)$ (i.e. $\mu(t)$ increases with time)

defines type I, and a decelerating decay (i.e. $\mu(t)$ decreases with time) type III survivorship [10].

Human mortality statistics are generally reported as number of deaths in a certain population occurring *per year* and *per 1000* or *per 1 million* of that population. The corresponding hazard function in this literature is usually called the death-rate, or simply mortality rate, and it is often shown as a function of age. The exponential rise of this rate, observed from an age of about 15 onwards, is referred to as the Gompertz law [11].

3 Incandescent light bulbs as a model of infant mortality

Studies of mortality enable observation of both short and long-term effects arising from congenital abnormalities[4]. Thus it is tempting to attempt a reverse analysis and derive information about the defects from the death rate curves. Here we examine how this can be done using a simple model for incandescent light bulbs for which one has a fairly clear understanding of the failure process. To keep matters simple we assume only one type of defect is present. Our goal then is to connect the statistical distribution of these defects to the age-specific failure rate of a device.

3.1 Failure mechanisms

Light from an incandescent light bulb is produced by a filament heated to high temperature by an electric current passing through it. A common observation is that such light bulbs frequently fail when switched on. One route to failure may occur during the first milliseconds after the light is switched on, when the temperature of the filament can increase rapidly. This creates thermal expansion through which the filament is slightly distorted. If there is already a marked narrowing, the filament may then break. Another cause of failure is through the creation of a magnetic field. Again during the first milliseconds there is a high surge in current intensity due to the fact that resistivity of the tungsten increases with temperature. This creates a magnetic field which can deform the filament and break it at the most fragile place. This effect is reinforced when the filament is shaped as a coil forming a solenoid.

The resistance R of a filament of length L is given by $R = \int_0^L \rho(x)/s(x)dx$, where $\rho(x)$ and $s(x)$ are local material dependent resistivity and wire cross-sectional area, respectively. We will in the following discussion treat resistivity as a constant, $\rho(x) = \rho$, but allow for fluctuations in the cross-sectional area $s(x)$ along the filament.

[4] We include not only infant mortality but also adult mortality due to long-term consequences of congenital mortality. For instance, it is known that heart defects have often a delayed effect.

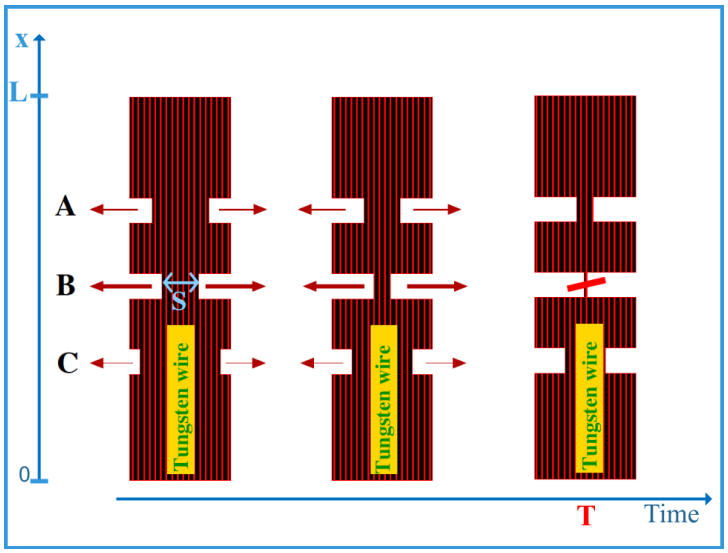

Fig. 1 Simple model for the thinning and eventual breaking of a tungsten filament in a light bulb due to the flow of an electrical current. Since the local resistance of the filament increases inversely with the local cross-sectional area, there will be greater heat release at narrow sections. This in turn leads to greater local evaporation of tungsten (called *filament notching* and indicated by the horizontal arrows), eventually leading to the failure of the filament at the narrow section. Note that only the smallest local cross-section, S, that is to say the most serious defect, plays a role in this process. T denotes the time of failure, which is also the lifetime of the light bulb.

A smaller local cross-section $s(x)$ will result in a local increase in resistance dR, and greater heating, which increases the local temperature. (The effect would be even more enhanced had we allowed for an increase in resistivity ρ with temperature in our model.) Around this hot spot the evaporation of tungsten will be faster than across the cooler regions. This will eventually lead to the severance of the filament and failure of the lamp (see Fig.1). In the simple model considered here it is the *smallest* value of $s(x)$ along the filament which will be responsible for the failure, and we denote this by $S = \min[s(x); 0 \leq x \leq L]$.

3.2 Connection between lifetime and severity of the defect

The time to failure depends upon the degree to which sections of the filament are reduced prior to initial use. This implies there is a one-to-one relationship

$$T = g(S) \tag{5}$$

between the smallest cross-sectional area, S, and the failure time T of the filament (and thus bulb). In principle, $g(S)$ can be obtained from a fairly simple model involving physical relationships related to heating, evaporation

and electrical resistance. Conversely, one could infer the minimum cross-section from knowledge of the failure time.

3.3 Relation between distribution of defects and distribution of lifetimes

Considering now an ensemble of light bulbs, a probability density distribution $f_S(S)$ of minimum values of cross-sectional area S, as defined above, translates into a probability density $f_T(T)$ of bulb lifetimes T.

In the simplest case, all bulbs have the same value of S and thus they will all fail at the same time, say T_1. Thus the probability density $f_T(T)$ (also called failure density function, see section 2) will be zero up until T_1, where there will be a spike (δ-function). For times exceeding T_1, $f_T(T)$ will again be zero.

In the general case, given a probability density $f_S(S)$ of minimal cross-sections, the fundamental transformation law of probabilities states that

$$f_T(T)\delta T = f_S(S)\delta S. \tag{6}$$

The probability density for the smallest cross-sectional areas is then determined from the failure density function $f_T(T)$ as

$$f_S(S) = f_T(T)g'(S), \tag{7}$$

where we have used $\frac{\delta T}{\delta S} = dg/dS = g'(S)$, from eqn.(5).

Thus knowing the probability density of the failure times we can in principle compute the probability density of the defects, and *reverse*.

Let us consider the simple case of a linear function $g(S)$, i.e. $T = g(S) = aS + b$, where $a, b > 0$, and a uniform distribution of minimal cross-sections, i.e. $f_S(S)$ is constant, within the interval $[S_1, S_2]$, see Fig. 2. From $f_T(T) = f_S(S)/a$ it follows that the failure times are also uniformly distributed within the interval $[T_1, T_2] = [aS_1 + b, aS_2 + b]$. Thus for this sample of bulbs there will be no failures up to the time T_1 where the first failure will occur. More failures will follow with a constant frequency until time T_2 when every member of the sample will have failed [5]. It can be used for any device whose lifetime is determined by a single parameter and we use it in Section 4.3 (in a modified form) for soap films confined in tubes of various lengths.

The argument can also be generalized to cases where the lifetime is determined by more than one parameter.

What makes this argument important here is that it connects what we can observe and measure, namely the age-specific death rate, to the birth defects. **Written in terms of the reliability/survival function $s(t)$, Eqn (7) is expressed as**

$$f_S(S) = -g'(S)\frac{ds(t)}{dt}, \tag{8}$$

[5] This is indeed what one observes for fish mortality in the yolk sac phase [12].

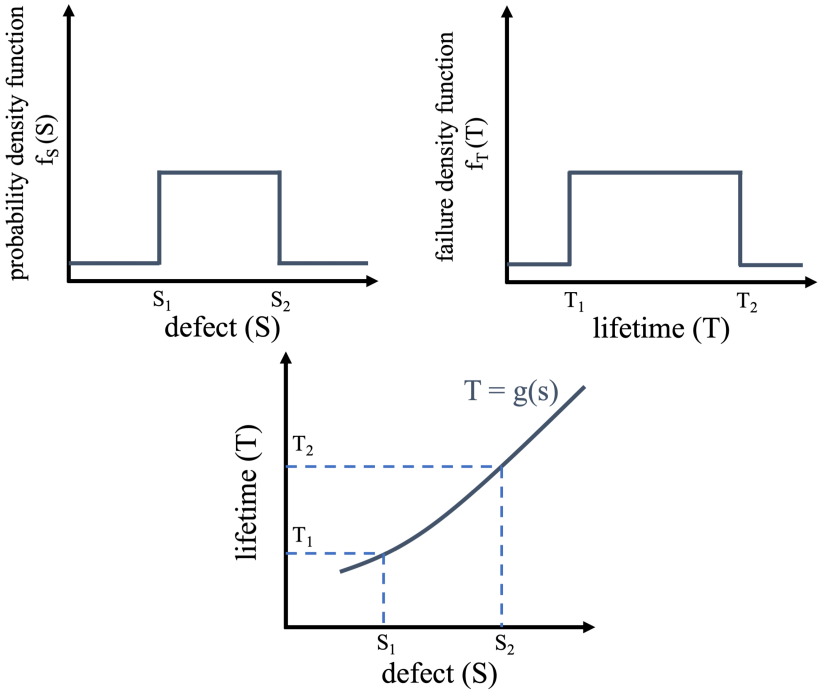

Fig. 2 Relation between probability density function $f_S(S)$ of defects S, failure density function $f_T(T)$ of lifetimes T, and function $T = g(S)$, linking defect size to lifetime. Knowledge of any two of these relations allows for the computation of the third. For the illustrative example of light bulb failure discussed in the text we have chosen a rectangular distribution for $f_S(S)$, where the defect S corresponds to the minimal cross-section of the filament (Fig.1). In section 4 we will construct a distribution $f_T(T)$ from lifetime data for soap films, using Eqn (8).

where we have used Eqn (3). It is in this sense that infant mortality gives us an insight into the internal working of a device or organism. In the next section we will demonstrate the application of Eqn(8) for experimental data for the lifetime of soap films.

4 Using soap films for the study of failure

Thin liquid films, stabilized by surfactants, may be used as a simple physical system for an experimental study of the statistics of failure [13, 7]. Here the lifetime is defined as the time between the creation of a film out of a surfactant solution and its eventual rupture, which is, in many cases, brought about by statistical thermal fluctuations.

The lifetime of such films, commonly called “soap films”, is thus a well defined quantity. A film either exists or has vanished; there is no in-between

state. This, together with the simple and cheap experimental set-up, makes such films a suitable experimental system for the study of failure. This was previously explored by [7,13], who studied *ensembles* of 10-20 films which were placed equidistantly in (sealed) vertical glass or perspex cylinders. Data for over 4000 films showed that for this set-up, which allowed for film interactions in the cylinders, the long term failure/mortality rate is best described by an exponential increase in time (Gompertz law, see section 2).

Here we have studied lifetimes of *individual* films under a variety of different experimental conditions. For example, we placed the films in glass cylinders of different lengths or cross-sectional area. This resulted in a number of empirical relationships for the *average* lifetime, $\langle T \rangle$, as a function $g(S)$ of these 'control parameters' which here we denote by S, since in the context of the above discussion they take on the role of lifetime defining 'defects'. The requirement to use the average film lifetime is due to the substantial role that fluctuations play in film stability (see the discussion below).

Using the relation,

$$\langle T \rangle = g(S), \tag{9}$$

together with the failure density function $f_T(T)$ obtained from our experimental data, will allow us to identify the underlying 'defect' distribution $f_S(S)$ using the mathematical framework developed above, c.f. Fig.2.

4.1 Ageing of a soap film

Over the course of its lifetime a surfactant-stabilized liquid film experiences several stages of aging which are generally well understood within the framework of physics and physical chemistry [14,15]. However, an understanding of the final stage, i.e. the detailed mechanism of film *rupture*, is still limited [16]. The thickness of a freshly formed film ranges between 1 to 100 microns [17], but it is rapidly reduced due to the drainage of liquid out of the film. In thick vertically displayed films, gravity plays an important role in establishing a vertical gradient in thickness. But, as in the case of horizontal films, capillary action is the key driver for film thinning. The timescale for this process is set by both bulk and surface viscosity of the surfactant solution [14], together with film orientation.

Once the local film thickness has decreased to about 100 nm, drainage is slowed down, as eventually the attractive Van der Waals forces on the opposing sides of the film are balanced by steric and electrostatic repulsion due to the presence of surfactant molecules. This is accompanied by the formation of small areas ("spots") on the film which appear black in reflection and are indicative of a thickness of less than about 30 nm (common black film). These black spots grow in size and merge, resulting in a liquid film which appears completely black in reflection. Evaporation may reduce the film thickness even further, down to about 5 nm (Newton black film)[17]. Such films are metastable, but they ultimately rupture, as thermally induced thickness fluctuations may result in the formation of a hole which rapidly grows in size. Evaporation is seen to

play a significant role for film stability in this regime [18] and film lifetime increases with relative humidity [19].

Film rupture may also be triggered via the deposition of particles onto the film or the addition of anti-foaming chemicals which reduce or replace the amount of surfactant at the interface. The former mechanism might play a role in our experiments described below since they do not take place in a dust free environment. This would be a further support of the view that film rupture should ultimately be seen as a stochastic process [16].

4.2 Experimental set-up

All our experiments were performed at room temperature using solutions made from sodium dodecyl sulfate (SDS, purity $\geq$90%, purchased from Sigma-Aldrich), dissolved in Millipore water at a concentration of 10.1 g SDS to 290 mL water. The solutions were freshly prepared for each experimental run, using a magnetic stirrer for about 30 minutes. Temperature was monitored for some experiments but we could not detect any influence on average film lifetime for the fluctuations in the laboratory temperature, which were about $\pm 1.5^o$C.

We used sets of glass tubes of three different lengths (L = 3cm, 10cm, 20cm) and diameter 1.6 cm which we sealed with one or two standard laboratory rubber stoppers. The tubes were cleaned and then dried before each experimental run.

An individual liquid film was created by dipping a tube perpendicularly into the SDS solution and then withdrawing it. Each of our tubes contained only one film, placed in its middle; see the schematic in Fig. 3(a).

The tubes were monitored using a digital video camera (AVT Marlin F131B) connected to a PC, with images being recorded every 6 seconds. We found it convenient to image a row of 12 parallel aligned tubes in one experimental run; when using short tubes, as shown in Fig.3(b), it was possible to record two such rows (corresponding to two experimental runs) in one session. The lifetime of each film was determined from visual inspection of the recorded images and taking the time-stamp of the last image at which a film was still present in the tube.

4.3 Results

The data presented and analyzed below is for a total of $5 \times 144 + 1 \times 132 = 852$ films, contained in tubes of width 1.6cm and length 3cm, 10cm and 20cm, respectively. The tubes were placed vertically, i.e. all films were oriented horizontally. In one set of experiments the tubes were sealed with rubber stoppers at both ends, in the other set the stopper was inserted only at the bottom end.

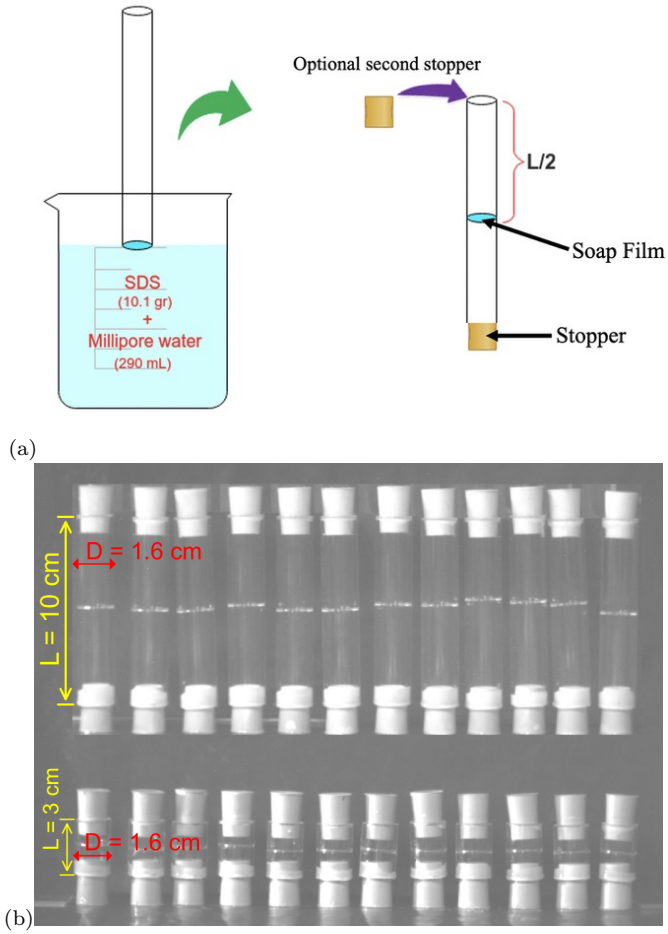

Fig. 3 Experimental set-up. (a) Liquid films were created by dipping glass tubes of three different lengths (and for the data presented here, with diameter 1.6cm) vertically into an aqueous SDS solution and then withdrawing them. At this stage the films are free to slide along the tube wall and can be brought to the centre of the tube. Sealing the tube at the bottom end using a rubber stopper then fixes the film position. Experiments were also carried out where the tubes were sealed with two stoppers. (Dimensions of the conical stoppers: length 2.4 cm: max. and min. diameter 1.5 cm and 1.8 cm). (b) Photograph of the set-up for an experimental run featuring 24 vertical tubes of two different lengths, sealed with two stoppers, and containing one film each. The horizontal films appear as thin bright lines.

Figure 4 shows that the average lifetime $\langle T \rangle$ of a film increases approximately linearly with the length L of the tube in which it is contained, i.e.

$$\langle T \rangle = g(L) = T_0 + cL, \tag{10}$$

where the fit parameters c (dimension: time/length) and T_0 (dimension: time) were determined using linear regression. (An offset T_0 was included in the fit

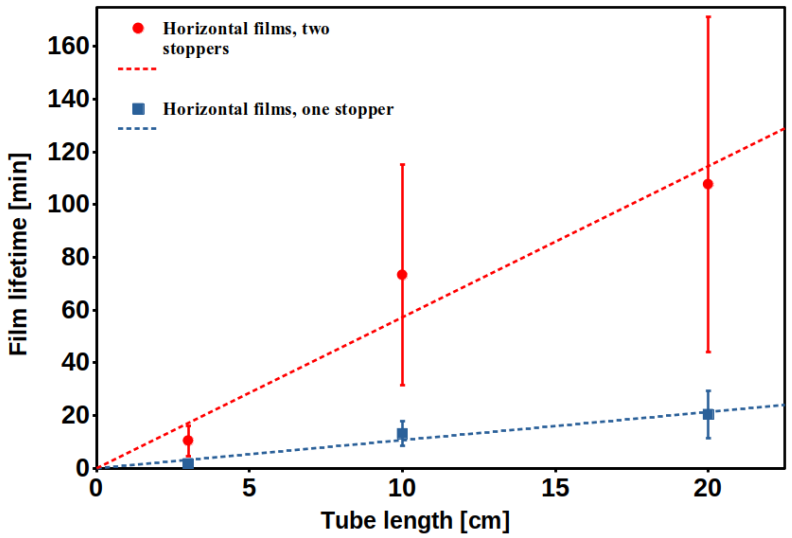

Fig. 4 The average lifetime $\langle T \rangle$ of a liquid film enclosed in the centre of a tube varies roughly linearly with the tube length L. Sealing the tube at both ends leads to a large increase of average film lifetime, in comparison to sealing it only at the bottom end. Each data point is the average over 144 measurements; the fluctuations are substantial (coefficient of variation $C_V \simeq 0.6$ in the case of two stoppers; $C_V \simeq 0.4$ in the case of one stopper). Linear regression leads to slopes $c = 1.08$ min/cm (one stopper) and $c = 5.57$ min/cm (2 stoppers), with corresponding offsets $T_0 = -0.09$ min and $T_0 = 2.56$ min.

since it is possible to maintain a film at finite lifetime even in the limit where a tube is shortened to just a ring. Note, however, that in the analysis that follows, only the value of the slope c is of relevance.)

Before moving on with our analysis we need to comment on the possible origin of this linear relationship of Eqn (10). We find that it is valid also for a number of variations of the set-up described here, involving tubes that were placed horizontally or vertically, sealed with two or one stoppers, or even not closed at all. The range of average lifetimes differs in all these different sets of experiments, however, the linear dependence on tube length remains, although with different values for the constant c. (The details of these findings, based on a total of $15 \times 144 = 2160$ films, will be discussed elsewhere.)

What is the origin of the linearity? In unsealed tubes there clearly is a (roughly linear) gradient in humidity along the tube, as it varies from 100% at the film location to its ambient value at both tube ends. As commented above, evaporation plays a major role for film stability, and evaporation is driven by humidity gradients. The longer the tube, the smaller the gradient will be, which should in turn lead to longer lifetimes.

We assume that such gradients also exist in tubes that are sealed (the quality of the seal was confirmed by probing for leakage when immersing a sealed tube in water); also in this case humidity will be 100% at the film and

decrease away from it to some finite value, in this case generally higher than that outside the tube. The argument for obtaining an increase in film lifetime by having longer tubes is thus as above.

Clearly average film lifetimes cannot increase indefinitely with tube length and we expect it to level off eventually, making other factors the most relevant ones for film rupture.

Let us stress here that we do not claim to have a full understanding of both origin and possible breakdown of the linearity. However, for the following discussion the *origin* of the linearity is not key. It is rather the *existence of an empirical law* for average film lifetime as a function of tube length which is required to make a prediction of the distribution of tube lengths from measurements of the lifetime of the films they contain.

We will for the following analysis represent our data in terms of the survival or reliability function $s(t)$ introduced in section 2.

From our data for the lifetime of individual films we can construct a time series $N(t)$, where $N(t)$ is the number of films that are still intact at time t. The survival function is then computed as $s(t) = N(t)/N(t = 0)$ (Eqn 1).

The initial number of films was $N(0) = 144$ in all but one of our different types of experiments (in the one-stopper experiment for the 10 cm tube $N(t = 0) = 132$). Note that $s(t)$ decreases whenever one (or more) films rupture at time t. Fig. 5 shows that in both our one and two stopper data an initially very slow decay of $s(t)$ away from $s = 1$ eventually gives way to a rapid drop, before the decay slows down again until all films have ruptured, i.e. $s = 0$.

In order to test whether information on the distribution of tube-lengths (in our case three δ-functions with peaks at $L = 3cm, 10cm, 20cm$) can be obtained from an analysis of film lifetime data for the one or two stopper experiment we have proceeded as follows. Our starting point will be the *aggregate* of the three survival functions, shown in Figs. 6 (a) and 7 (a). We have employed some smoothing to the data by grouping it into bins along the time axis. We have also applying a time-weighting that takes into account the times within each bin at which $s(t)$ changes its value. Furthermore we have chosen bin sizes that increase linearly with time to account for the fact that more film ruptures occur at earlier times.

Knowledge of the reliability function $s(t)$ allows for the computation of the failure density function $f_T(t) = -ds(t)/dt$ (Eqn (3)). The derivative was obtained numerically from our binned data for $s(t)$ (Figs. 6 (a) and 7 (a)) using the central difference method.

When considering our simple model for light bulb failure, with its one-to one relationship between lifetime T and minimal cross-section S, the distributions $f_T(T)$ and $f_S(S)$ were directly related via eqn.(7). In the case of our soap film data we only know the variation of the *average lifetime* $\langle T \rangle$ with tube length L. We argue that in this case the distribution $f_L(L)$ is *approximately* given by

$$f_L(L) \simeq \frac{d\langle T \rangle}{dL} f_T(T) = -\frac{d\langle T \rangle}{dL} \frac{ds(t)}{dt}. \tag{11}$$

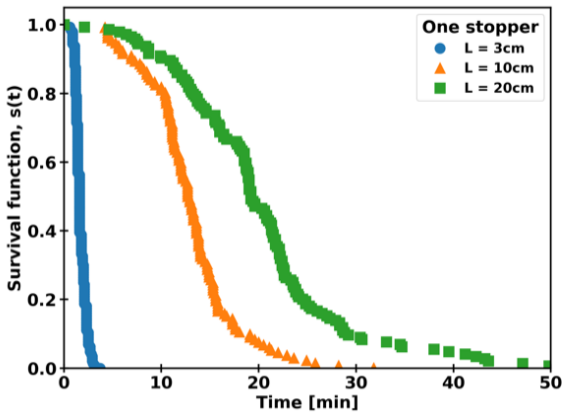

(a)

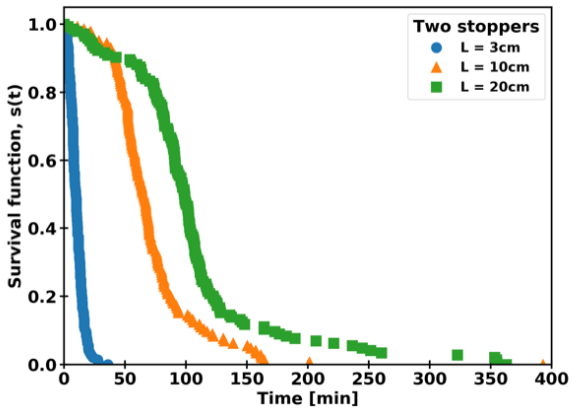

(b)

Fig. 5 Variation of survival/reliability function $s(t)$ as a function of time for films in tubes of length 3cm, 10cm and 20cm, respectively. Note that the lifetimes of the films in the tubes sealed with two stoppers (Figure b) greatly exceeds those in tubes sealed with only one stopper (Figure a). This highlights the effect of evaporation. The initial number of films in each of the different types of experiments was $N(t = 0) = 144$, apart from the one-stopper data for the 10 cm tube, where $N(t = 0) = 132$.

Similarly to the treatment in proportional hazard models [20] we have empirically identified a covariate, or risk factor (in our case the tube length) which is multiplicatively related to the 'hazard'. As in a so-called semi-parametric model, the mean response in our population of films, namely the average film lifetime, depends linearly on the covariate.

We have also computed the coefficient of variation (ratio of the standard deviation of $f_T(T)$ to its mean $\langle T \rangle$) and find that it is independent on tube length (although it differs between the two-stopper and the one-stopper data).

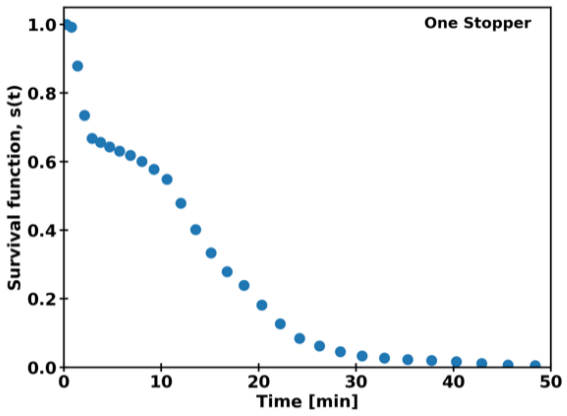

(a)

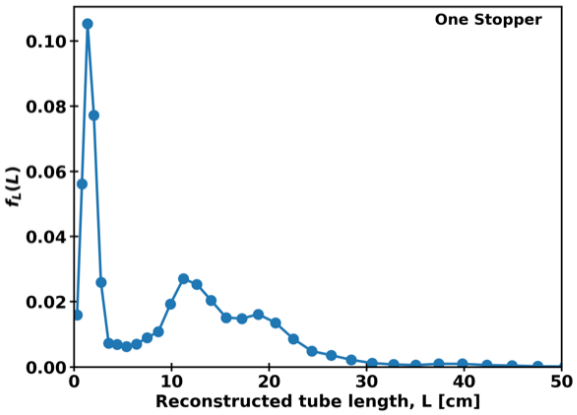

(b)

Fig. 6 (a) Survival function $s(t)$ for a combined and smoothed data set of $132 + 144 + 144$ films placed in tubes of three different lengths (3cm, 10cm and 20cm) closed with only *one* stopper (c.f. Fig. 5 (a)). (b) Reconstruction of the distribution of tube lengths using the methodology described in the main text, Eqns (11) and (12). The three discernible peaks at around 2cm, 11cm and 19cm correspond to the three different lengths of the tubes used in the experiments.

The mean lifetime $\langle T \rangle$ may thus be taken as a first approximation to the distribution $f_T(T)$. The distribution function itself is independent on the specific set of lifetimes we observe in our experiment. Were we to repeat the experiment we would observe a different set of lifetimes but the distribution function $f(T)$ would be unchanged.

From eqn.(11), and use of eqn.(10), we then obtain

$$f_L(L) \simeq c f_T(T), \tag{12}$$

where the constant c is determined by linear regression, see Fig. 4.

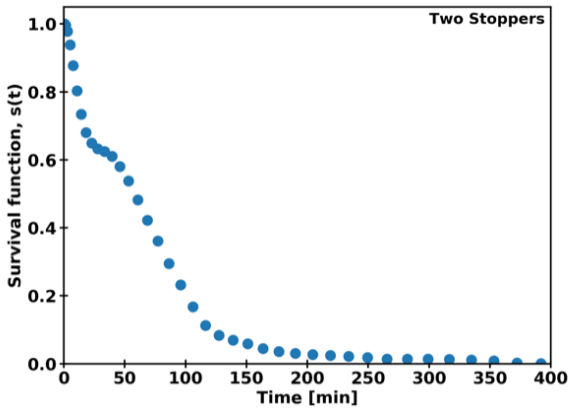

(a)

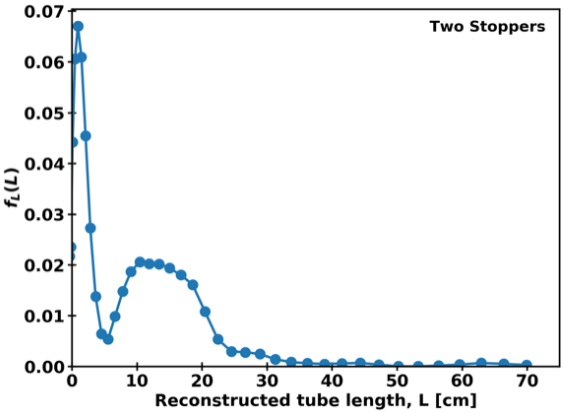

(b)

Fig. 7 (a) Survival function $s(t)$ for a combined and smoothed data set of 3×144 films placed in tubes of three different lengths (3cm, 10cm and 20cm) sealed with *two* stoppers (c.f. figure 5 (b)). (b) Reconstruction of the distribution of tube lengths using the methodology described in the main text, Eqns (11) and (12). There is a sharp peak at $L \simeq 2$ cm and a broad peak between about 8cm and 22cm. Our data for the two-stopper experiment is thus not of sufficient quality to differentiate between the 10cm and 20cm tubes used in the experiments.

The results of applying eqn.(12) are shown in Figures 6 (b) and 7 (b), which display the computed distributions $f_L(L)$ for respectively one and two stopper data. Conversion of the time-axis into a length-axis is via $L = (\langle T \rangle - T_0)/c$.

In the case of our one-stopper experiment the distribution $f_L(L)$ clearly indicates the presence of three dominant tube lengths of about 2cm, 11cm and 19cm (which might serve as a further justification of eqn.(11)). For the two stopper experiment only two peaks can be identified, one of which is very broad, i.e. the inherent noisiness of the data makes it impossible to resolve

film ruptures in the 10cm tube from ruptures in the 20cm tube. Figure 5(b) shows that this is due to the time interval from about 75 to 90 minutes where both film populations suffer from increased rupturing.

Let us note that our data sets are quite limited in size, our sets of 144 films for each experiment type are much smaller than what was used in previous studies which involved collections of film in tubes [13, 7]. (The lifetime data for fluorescent lamps mentioned earlier is based on an even smaller number of only 36 lamps [4].) Presumably a larger number of films would reduce noise, resulting in a smaller coefficient of variation than what we obtained here ($C_V \simeq 0.6$ in the case of two stoppers data; $C_V \simeq 0.4$ in the case of one stopper data).

Despite these current limitations our analysis presented in **Figures 6 and 7 has demonstrated that it is possible to induce a distribution of tube lengths, $f_L(L)$, from statistical lifetime data, $f_T(T) = -\frac{ds(t)}{dt}$. The necessary requirement for this is a relationship between average lifetime and tube length, i.e. the relationship shown in Fig. 4. We have thus provided an example, using experimental data, of the procedure introduced in Section 3.3 for light bulbs, as illustrated in Figure 2.** We have had similar success also for our analysis of vertical films, confined in horizontally placed tubes (to be presented elsewhere).

Lifetime data for biological systems is generally presented in terms of a death rate (failure rate), $\mu(t)$, as was introduced in section 2, Eqn (4).

Figure 8 shows $\mu(t)$ as computed from the one-stopper data in the case of the 20 cm long tube shown in Fig. 5. An initial roughly exponential increase of $\mu(t)$ levels off after about 20 minutes and gives way to fluctuations about a roughly constant value. We find qualitatively similar behaviour also for our other data sets, not shown here. Again there is an exponential increase in the failure rate, i.e. the form associated with the Gompertz law for human mortality [11] or a Type I survival function in ecology (see Section 2). This is similar to the findings by [7] for the case where multiple films were confined in tubes.

In Fig. 9 we show the failure rate computed for the *combined* data sets for tubes with only one stopper (cf. Fig. 5(a)). **In the same figure we also plot the percentages of the films contained in the 3cm, 10cm, and 20cm long tubes, respectively.**

The initial sharp rise in the failure rate $\mu(t)$ corresponds to the rupturing of the films contained in the 3cm long tubes. These have the shortest lifetimes and have all vanished after about 3 minutes (c.f. figure (5a)). As their presence in the combined film population decreases, the failure rate steadily decreases. It only begins to rise again after about 6 minutes, when the first films in the 10cm long tubes begin to rupture. As the rate of these rupturing events slows down at about 12 minutes the failure rate is again seen to decrease once more. However, there is now increased film rupturing also of films in the 20cm long tubes, making this second minimum in the failure rate at about 17 minutes much shallower than the first one.

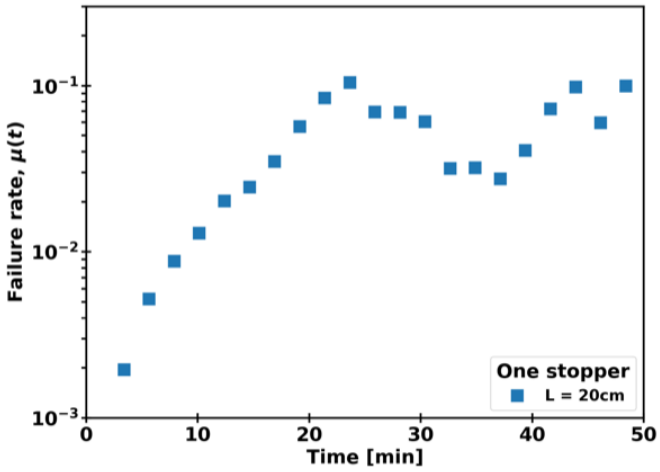

Fig. 8 Time-dependent failure rate/hazard function $\mu(t)$, eqn.(4), for films contained in tubes of 20 cm length, closed with only one stopper. Up to about 25 minutes the failure rate increases roughly exponentially, before fluctuating around a constant level. The size of the fluctuations reflects the very small number of remaining films, cf. the corresponding survival function $s(t)$ shown in Fig. 5(a).

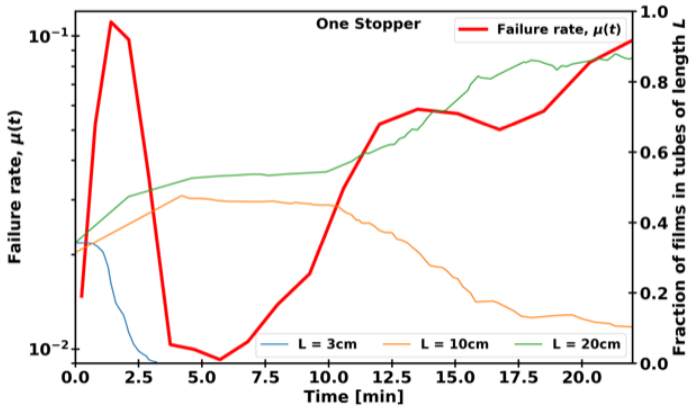

Fig. 9 Failure rate $\mu(t)$, eqn.(4) and fraction of films in tubes of length 3cm, 10cm, and 20cm, as a function of time. $\mu(t)$ was computed from the combined survival functions $s(t)$ for films confined in tubes with one stopper, see Figure 6(a). The 'double bath-tub shape' is due to the different average lifetimes of films contained in tubes of three different lengths. To avoid large fluctuations when computing $\mu(t)$ we only show data for the first 22 minutes. At this stage 86% of the initially 320 films have ruptured.

The failure rate data for the combined data set for tubes with two stoppers, Fig. 5(b), is similar, but does not feature the second minimum.

Figure 9 thus illustrates what is called the "bath-tub" curve of failure rate, known for example from data for technical devices. Defective samples (in our case represented by films that are confined in short tubes) lead to an initially high failure rate, which begins to decrease once the samples have stopped working (i.e. the corresponding films in the short 3cm tubes have ruptured). In Figure 9 we also see a second, shallower "bath-tub"; as we have remarked in the introduction, information about the defect distribution can be inferred from lifetime data.

We will in the next section present a similar graph concerning the variation of human mortality rate due to the presence of the congenital defect of aorta narrowing.

5 A human congenital defect: aortic narrowing

As noted at the outset, the major focus of this and previous papers [2,3] is to study the connection between initial abnormalities (whether from manufacturing or congenital anomalies) and subsequent death rates. Of importance is the determination of the delay between introduction of a defect and the resulting failure which may occur after a substantial time lag. For light bulbs the time interval between "birth" and "failure" may typically be a few years whereas for soap films the time lag is only a matter of (tens of) minutes. For the case of heart valve narrowing, the time lag between birth defect and death can be as long as 70 or 80 years. At first sight it seems difficult to imagine how the death say of a 75-year old person can be traced back to a birth defect. Here we explain what makes this possible. Moreover, we show that the order of the change in magnitude of the infant death rate for this specific cause of death is consistent with the frequency data for severe aortic stenosis or narrowing.

First, let us describe how heart valves work. The human aortic valve is located at the point where the aortic artery (the largest artery in terms of flow rate) is connected to the heart, more precisely, to the left ventricle of the heart. Normally, the valve consists of 3 leaflets with an opening of approx. 3 cm^2. When the ventricle contracts, it forces blood through the valve into the aorta. Then, when the ventricle expands again, the valve closes and prevents blood flowing backwards. In this way the valve acts exactly like that in a pump.

In a patient with aortic valve stenosis, the opening of the valve has narrowed. This can occur for two different reasons: (i) a birth defect where instead of having 3 leaflets, the valve has only 2 leaflets or, less often, only one leaflet. The three cases are depicted in the inset of Fig. 10. (ii) Even without such a birth defect the valve may become narrow due to ageing from calcification (just like calcification or 'furring' which occurs in water pipes or washing machines over time). Here we focus mainly on the first situation.

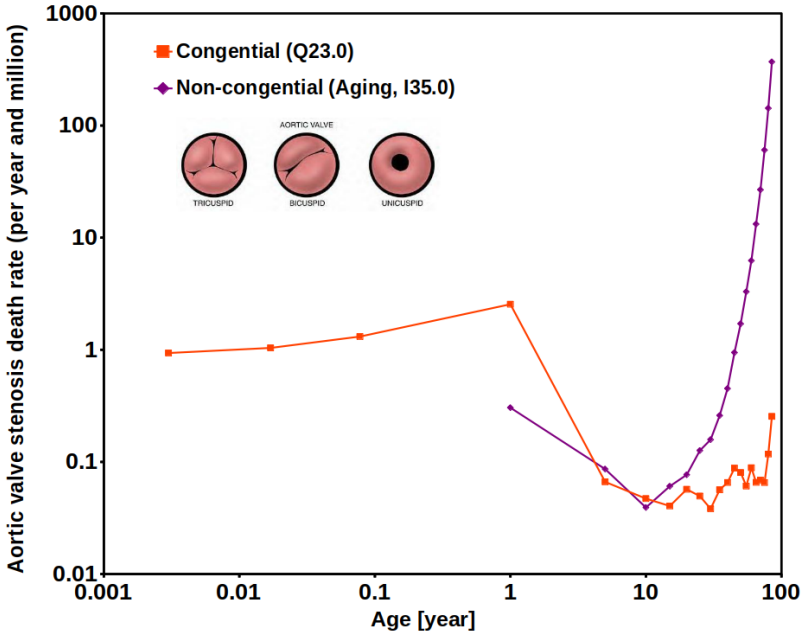

Fig. 10 Death rates for aortic valve narrowing: congenital versus non-congenital. In the 10th International Classification of Diseases (ICD-10) the codes are Q23.0 for the congenital case and I35.0 for the non-congenital case. There is a strong decline of the death rate between one year after birth and an age of about 10 years. In the text, we argue that this decline is due to cases of severe stenosis which will lead to short lifetimes of the children. In the cases of mild aorta narrowing, the lifetime can be several decades. The inset shows the three possible shapes of the valve: left is the normal 3-leaflet valve, whereas the two others are abnormal 2- and 1-leaflet shapes. (Source of data: CDC WONDER [21], February 2020.)

Quite understandably, the area of aortic valves varies also with body size. In order to scale out this dependence the so-called AVAi index is defined as the ratio of aortic valve area (AVA) to body surface area. AVA values for adults [6] ranges from 0.4 cm^2 to 4.5 cm^2, whereas the body surface area of typical adults is $\sim$ 2 m^2. The AVAi therefore ranges from $0.2 \leq i \leq 2.2$ cm^2/m^2. Values below 1.1cm^2/m^2 indicate that there is a form of stenosis, with severe stenosis corresponding to an index below 0.4 cm^2/m^2[22][7]. For these situations death happens fairly quickly (typically within a few weeks or months). Above the optimal value additional risks arise, for example regurgitation, when instead of closing completely, the valve allows blood to flow in the opposite direction.

[6] The source is: https://e-echocardiography.com/page/page.php?UID=1867001

[7] We could not find corresponding AVAi values for children.

5.1 Cascade of processes generated by an aortic narrowing

As a consequence of the narrowing, ventricle contractions must generate a higher pressure in order to move blood forward into the aorta. This added pressure, termed the valve gradient, can reach 6 mmHg or $\sim$ 800 Pa. This added pressure is a remarkable feedback effect without which the negative consequences of stenosis would become apparent much earlier. Nevertheless, however favourable this may be in the short term, this compensatory response has two unwelcome implications. (i) Thickening of the muscular wall results in loss of flexibility of the ventricle which impairs pump efficiency. (ii) Greater muscular activity requires more oxygen which may deprive other essential organs. Foremost of these is the brain, and syncope or loss of consciousness becomes a possible symptom. Naturally, the oxygen need becomes more acute when efficacy of the lungs also decreases due to ageing. In short, there is a bound due to the extra costs and risks of this response that depends on the level of physical activity. Dynamic measurements performed during physical activity of the patient show symptoms which at rest become visible only many years later.

The previous situation is a rare example where one has a good understanding of the whole process from congenital malformation to death. Moreover, once one knows the physiological mechanisms involved, it is hardly surprising that the whole process may play out over several decades.

The age-specific death rates for the congenital and pure aging processes are shown in Fig. 10. Infant mortality is largely dominated by the first process, whereas old age mortality is dominated largely by the second. Around age 70-80 about 100 times more deaths due to ageing are reported than deaths due to initial birth defects. But are these small numbers reliable? How do doctors who fill in death certificates differentiate between the overwhelming 'normal' deaths and the small number of deaths due to congenital birth defects? Diagnosis is possible in this example, owing to the geometric character of the aortic valve. Does it have 3, 2 or 1 leaflets? Naturally, there are also a few 3-leaflet cases which are affected by birth defects. These will be more difficult to identify in old age. So the old age congenital data shown in the graph may be somewhat underestimated.

5.2 Congenital infant mortality vs. defect frequency

Investigation of the connection between death rate and defect frequency is an interesting exercise because these are two very different kinds of data. First, we explain how they are measured.

Infant mortality rates come from death certificates which rely on medical assessments. The congenital aortic valve disease is labeled Q23.0 in the 10th International Classification of Diseases. During the infant phase, i.e. under the age of one year, one expects few mistakes because death due to ageing (I35.0 in the same classification) is essentially non-existent. According to Fig. 10,

shortly after birth, the death rate is roughly constant at about 1 and 10 per year per million. However, there is a sharp decay after about one year with the death-rate due to congenital stenosis dropping by nearly two orders of magnitude in the following years. The minimum is at about 10 years with less than about 0.1 deaths per year and million. In the following we will argue that the large drop is due to infants with the most severe forms of stenosis who will for this reason have a very short life-span.

Eroğlu *et al.* studied the natural course of AVS for a total of 388 patients suffering from this condition [23]. The severity of the defect was reported in terms of the maximum peak systolic instantaneous gradient in aortic valve pressure, as determined using echocardiography. The findings were classified according to four different categories: pressure < 25 mmHg (trivial stenosis), 25–49 mmHg (mild stenosis), 50–75 mmHg (moderate stenosis), and > 75 mmHg (severe stenosis). The data was then divided into five different age groups, namely < 1 month, between 1 month and 1 year, 1.1 to 5 years, 5.1 to 10 years, and 10 to 20.6 years. In Fig. 11 we have used this data, taken from table 1 of [23], to plot distributions of severity of congenital aortic valve stenosis for these five different age groups.

What is striking in Fig. 11 is that the shape of the distributions clearly differs for the different age groups. One would expect the aortic valve area to increase for ages up to about 15 years, due to the overall growth of the patients, but this should not lead to a simple reclassification of the degree of severity. Note that when using AVAi values, as is often done when reporting data for adults, the effect of different body sizes is factored out.

In Fig. 12(a), which was produced from the same dataset as that of Fig. 11, we show the variation of the fraction of the different degrees of congenital stenosis (severe, moderate, mild, trivial, as defined in [23]), as a function of age[8]. We note that only the fractions of severe and moderate cases decrease with time and for this reason we show in Fig. 12(b) their combined fraction.

Eroglu *et al.* [23] carried out follow-up assessments of their patients after time spans ranging between one month, up to 21.6 years, however, the data provided in [23] does not distinguish for age groups in the results. The degree of aortic valve stenosis progressed in about one fifth of all patients, with the highest risk of progression in newborn babies and infants. Since patients with severe AVS are at an increased risk of sudden death [24, 25] we conjecture that it is this decrease of the severe and moderate cases of stenosis that leads to the decrease seen in the mortality rates up to age 10 as shown in Figure 10.

To support the conjecture we show in Figure 13 as a function of time both the death-rate data for congenital stenosis from Fig. 10 (left vertical axis) and the frequency of severe and moderate aortic stenosis (right vertical axis). We see that the death rate decays as the fraction of severe and moderate stenosis decays; furthermore, both data sets level off at about 10 to 20 years.

We note that for infants up to one year the mortality rate first increases slightly with age, before decreasing sharply. This effect is not seen in our data

[8] Note that such a Figure does not feature in the original paper by [23].

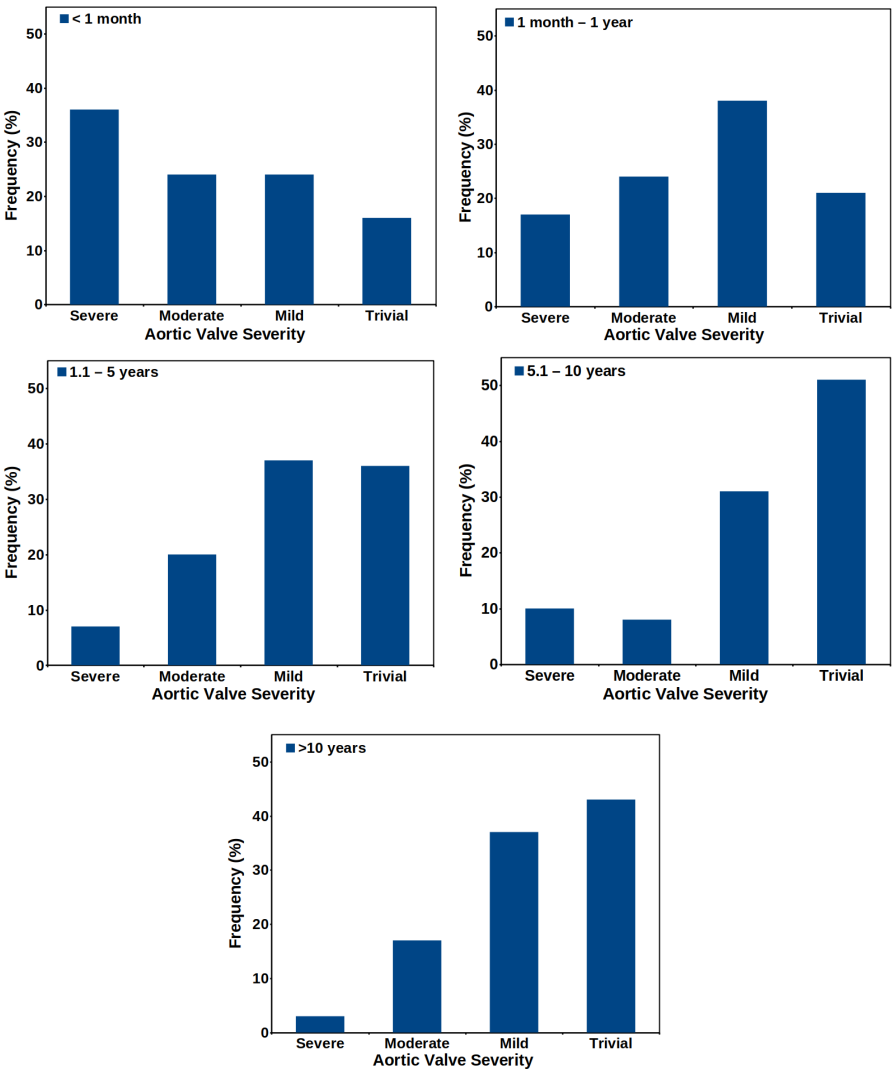

Fig. 11 Distributions of severity of congenital aortic valve stenosis. The data is for 388 patients (age range less than 1 month up to 20.6 years) [23]. Note the change in shape of the distributions. The data for infants and less than one-year old children features a high proportion of severe and moderate stenosis. In the age group 10 to 21 the percentage of severe stenosis is greatly reduced.

for AVS. However, this could be due to a time-lag, since even severe stenosis may not lead to an immediate increase in the mortality rate. We also see that the data for severe stenosis follows closer the mortality rate data than that of severe and moderate combined, in as much as it features a stronger decay.

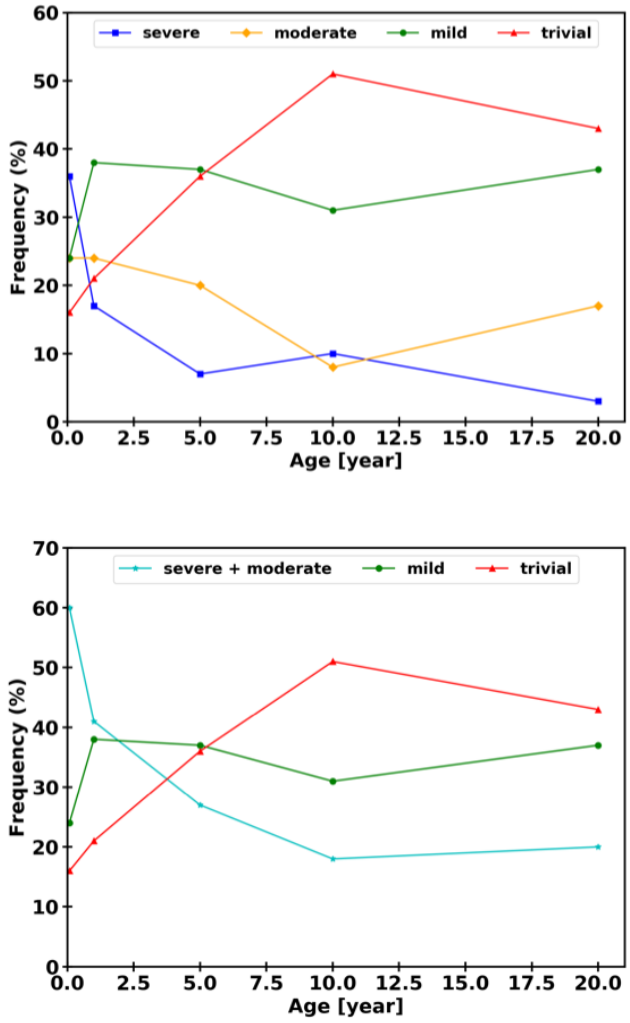

Fig. 12 Variation of the different degrees of severity of congenital aortic stenosis as a function of age group. (a) Since only the cases for severe and moderate stenosis decrease with time we show in (b) their combined contribution. Frequencies of both mild and trivial stenosis level to a roughly constant value after an initial rise. (Data taken from Table 1 of [23].)

Figure 13 is the equivalent graph to Figure 9, obtained from our soap film data. Both figures demonstrate a correlation between initial abnormalities (respectively, fraction of severe AVS or fraction of films in short tubes) and subsequent death rate variation.

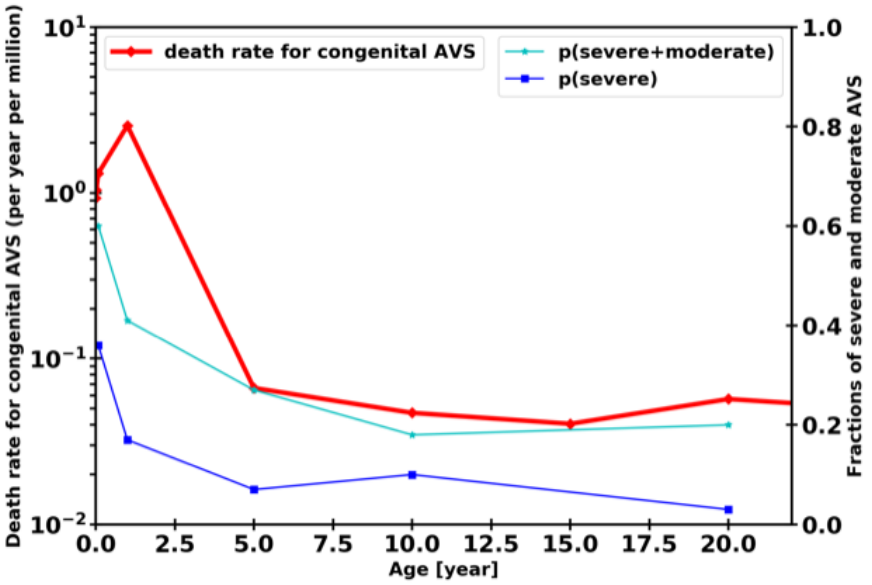

Fig. 13 Combined graph showing both the death rate due to congenital aortic valve stenosis of Fig. 10 (vertical axis: left) and the fraction of the occurrence of severe and moderate stenosis of Fig. 12 (vertical axis: right) as a function of time. There is a sharp decline for both severe stenosis data and death rate over the first five to ten years. (Original data from [21] and [23].)

6 Summary

The theoretical studies and empirical data presented here for three different systems, namely incandescent light bulbs, soap films and aortic valves show that it is possible to exploit survival and death rate data for an ensemble to gain insight into structural factors which control early-life mortality of individual members of the ensemble.

Using a simple model system for the lifetime of light-bulbs, we have argued in Section 3 that a defect distribution can be mapped into a distribution of bulb lifetimes, and *vice versa*. The requirement for this was the existence of a relationship between a characteristic of the light-bulb (i.e. the minimal filament cross-section) and the bulb lifetime.

In Section 4 we applied this approach to experimental data for the lifetime of soap films. Using an empirical relationship linking tube length to average film lifetime we were able to map survival functions into distributions of tube lengths (Figures 6 and 7).

Presenting the same experimental data in terms of a failure rate (mortality rate) $\mu(t)$ showed that its "bath-tub shape" variation 9

reflects the presence of defects, in this case films that were contained in short tubes.

In Section 5 we extended our approach to data from human biology. The initial decrease in mortality rate due to aortic valve stenosis is due the presence of severe cases of congenital stenosis which lead to a short life expectancy (Figure 13).

7 Outlook

Human mortality data continues to provide important information for the study of failure. This is partly due the large sample sizes, but also due to the long history of data taking; John Graunt's publication of detailed life-tables dates back to 1661. **In the book *Dynamics of Cancer* [26] S.A. Frank presents hundreds of data sets for the age-specific incidence of different types of cancers. Of particular note in the context of our study is the data for cancer in childhood. The observation that the details of the mortality curve reveals something about the underlying mechanism of the specific cancer type may be illustrated by the following two examples. The incidence with age of osteosarcomas increases during the time of rapid bone elongation; it decreases when bone growth has stopped in the teenage years. In contrast, the incidence of carcinomas, which is associated with epithelial cells, increases continuously with age, as this tissue renews itself throughout all ages.**

The identification of the relationship between defect size distribution and lifetime distribution which we discussed is also of relevance to the manufacturing of (semiconductor) devices [27]. Here it can be used to determine optimal burn-in parameters in order to ensure long lifetimes for the products leaving the factory.

In presenting this work we hope the reader is persuaded not just that there are analogies between inanimate and human systems, but that measures of mortality relate directly to the micro-structural nature of the system. Moreover, insights into mortality and disease in humans is directly linked to these microstructure elements and their organization.

In the case of early mortality [28], elements such as aortic valves are one such structural element. This presumably depends on genetics that determine the assembly process in the womb; mortality in later age can be linked to the strength of the immune system [29, 30].

8 Funding information

SH acknowledges funding from Science Foundation Ireland (SFI) grant 13/IA/1926. AI acknowledges funding from the Trinity College Dublin Provosts PhD Project Awards.

9 Conflict of interest

The authors declare that they have no conflict of interest.

References

1. M. Livi-Bacci. *A concise history of world population*. Blackwell Publishers, US, 1992.
2. A. Bois, E.M. Garcia-Roger, E. Hong, S. Hutzler, A. Irannezhad, A. Mannioui, P. Richmond, B.M. Roehner, and S. Tronche. Infant mortality across species. a global probe of congenital abnormalities. *Physica A: Statistical Mechanics and its Applications*, 535:122308, (2019).
3. A. Bois, E.M. Garcia-Roger, E. Hong, S. Hutzler, A. Irannezhad, A. Mannioui, P. Richmond, B.M. Roehner, and S. Tronche. Congenital anomalies from a physics perspective. the key role of manufacturing volatility. *Physica A: Statistical Mechanics and its Applications*, 537:122742, (2020).
4. Y. Ji, R. Davis, C. O'Rourke, and E. Chul. Compatibility testing of fluorescent lamp and ballast systems. In *IAS'97. Conference Record of the 1997 IEEE Industry Applications Conference Thirty-Second IAS Annual Meeting*, volume 3, pages 2340–2345. IEEE, (1997).
5. Illuminating Engineering Society of North America. *Lighting Handbook: Reference & Application*. Illuminating Engineering Society of North America, (2000).
6. M. Krajewski. The great lightbulb conspiracy. *IEEE Spectrum*, 51(10):56–61, (2014), https://spectrum.ieee.org/tech-history/dawn-of-electronics/the-great-lightbulb-conspiracy.
7. B. Haffner, J. Lalieu, P. Richmond, and S. Hutzler. Can soap films be used as models for mortality studies? *Physica A: Statistical Mechanics and its Applications*, 508:461 – 470, 2018.
8. S. Nee. Survival and weak chaos. *Royal Society Open Science*, 5(5):172181, 2018.
9. L.A. Gavrilov and G.N.S. The reliability theory of aging and longevity. *Journal of Theoretical Biology*, 213(4):527–545, 2001.
10. Sean Nee. Survival and weak chaos. *Royal Society open science*, 5(5):172181, 2018.
11. P. Richmond and B.M. Roehner. Predictive implications of gompertzs law. *Physica A: Statistical Mechanics and its Applications*, 447:446–454, (2016).
12. S. Berrut, V. Pouillard, P. Richmond, and B.M. Roehner. Deciphering infant mortality. *Physica A: Statistical Mechanics and its Applications*, 463:400–426, 2016.
13. S. T. Tobin, A. J. Meagher, B. Bulfin, M. Mbius, and S. Hutzler. A public study of the lifetime distribution of soap films. *American Journal of Physics*, 79(8):819–824, 2011.
14. E. Rio and A.-L. Biance. Thermodynamic and mechanical timescales involved in foam film rupture and liquid foam coalescence. *ChemPhysChem*, 15(17):3692–3707, 2014.
15. R.J. Pugh. *Bubble and foam chemistry*. Cambridge University Press, 2016.
16. D. Langevin. On the rupture of thin films made from aqueous surfactant solutions. *Advances in Colloid and Interface Science*, page 102075, (2020).
17. C. Isenberg. *The science of soap films and soap bubbles*. Dover Publications, New York, 1992.
18. L. Champougny, J. Miguet, R. Henaff, F. Restagno, F. Boulogne, and E. Rio. Influence of evaporation on soap film rupture. *Langmuir*, 34(10):3221–3227, (2018).
19. J. Miguet, M. Pasquet, F. Rouyer, Y. Fang, and E. Rio. Stability of big surface bubbles: impact of evaporation and bubble size. *Soft Matter*, 16:1082–1090, (2020).

20. D. Kumar and B. Klefsjö. Proportional hazards model: a review. *Reliability Engineering & System Safety*, 44(2):177–188, (1994).
21. Centers for Disease Control, Prevention, National Center for Health Statistics, et al. Underlying cause of death. *CDC WONDER. Published by the US Center for Disease Control and Prevention*, 2020.
22. J.T. Willerson, J.N. Cohn, H.J.J. Wellens, and D.R. Holmes. *Cardiovascular medicine*. Springer Science & Business Media, (2007).
23. A.G. Eroğlu, S.U. Atik, B. Çinar, M.T. Bakar, and İ.L. Saltik. Echocardiographic follow-up of congenital aortic valvular stenosis ii. *Pediatric cardiology*, 39(8):1547–1553, (2018).
24. D. Horstkotte and F. Loogen. The natural history of aortic valve stenosis. *European Heart Journal*, 9(suppl. E):57–64, (1988).
25. J.F. Keane, D.J. Driscoll, W.M. Gersony, C.J. Hayes, L. Kidd, W.M. OFallon, D.R. Pieroni, R.R. Wolfe, and W.H. Weidman. Second natural history study of congenital heart defects. results of treatment of patients with aortic valvar stenosis. *Circulation*, 87(2 Suppl):I16–27, (1993).
26. S.A. Frank. *Dynamics of cancer: incidence, inheritance, and evolution*, volume 1. Princeton University Press, 2007.
27. K.O. Kim, W. Kuo, and W. Luo. A relation model of gate oxide yield and reliability. *Microelectronics Reliability*, 44(3):425–434, (2004).
28. Q. Chen, Z. Di, E.M. García Roger, H. Li, P. Richmond, and B.M. Roehner. Magnitude and significance of the peak of early embryonic mortality. *Journal of Biological Physics*, pages 1–19, 2020.
29. BI Shklovskii. A simple derivation of the gompertz law for human mortality. *Theory in Biosciences*, 123(4):431–433, 2005.
30. P Richmond and B Roehner. *Acta Physica Polonica*, submitted to special issue incorporating proceedings of FENS 2019, 2020.